Observation of Magnetic Excitations of Skyrmion Crystal in a Helimagnetic Insulator Cu_2OSeO_3

Y. Onose,[1,2] Y. Okamura,[1] S. Seki,[1] S. Ishiwata,[1] and Y. Tokura[1,3]

[1]*Department of Applied Physics and Quantum Phase Electronics Center (QPEC), University of Tokyo, Tokyo 113-8656, Japan*
[2]*Department of Basic Science, University of Tokyo, Tokyo 153-8902, Japan*
[3]*Cross-Correlated Materials Research Group (CMRG) and Correlated Electron Research Group (CERG), RIKEN Advanced Science Institute, Wako 351-0198, Japan*

(Received 3 May 2012; published 20 July 2012)

We have investigated the low-energy dynamics of the triangular lattice of Skyrmions in a helimagnetic insulator Cu_2OSeO_3 in terms of microwave response. We have observed two elementary excitations of the Skyrmion with different polarization characteristics: the counterclockwise circulating mode at 1 GHz with the magnetic field polarization parallel to the Skyrmion plane and the breathing mode at 1.5 GHz with a perpendicular magnetic field polarization. These modes reflect the topological nature of Skyrmions and may play a central role in the Skyrmion dynamics.

DOI: 10.1103/PhysRevLett.109.037603 PACS numbers: 76.50.+g, 75.30.Ds, 75.85.+t

The concept of a topologically stable magnetic texture called a Skyrmion was first introduced in the field of nuclear physics [1], and then applied to the study of a quantum Hall ferromagnet [2] and cold atoms [3]. The crystallization of Skyrmions in magnets without inversion symmetry was also theoretically predicted more than two decades ago [4] and experimentally observed recently in chiral magnets such as MnSi and $Fe_{1-x}Co_xSi$ with use of the neutron diffraction and Lorentz transmission electron microscopy [5,6]. The Skyrmions in chiral magnets are quite mobile under electric current density as low as $\sim 10^6$ A/m^2 and in some cases, stable up to near room temperature [7–10]. These features imply the potential of practical application.

The Skyrmion is not only a nanoscale version of a magnetic bubble [11] but also characterized by a unique topological nature. As shown in Fig. 1(c), the direction of magnetic moment varies continuously and wraps all the solid angle in the Skyrmion. The topological nature affects the dynamics of conduction electrons in the Skyrmion crystal state and also the motion of the Skyrmion and induces emergent electromagnetic phenomena such as topological Hall effect, spin motive force, and Skyrmion Hall effect [9,12–15]. Similarly to the role of phonons in lattice dynamics of atomic crystal, the vibrations of Skyrmions should be essential for the low-energy dynamics of Skyrmion crystal. To study the effect of topology on such spin-vibrational modes, we have investigated the microwave response of Skyrmion crystal in a helimagnetic insulator Cu_2OSeO_3 with small Gilbert damping.

While the Skyrmion crystal has been observed so far mostly in the $B20$ transition metal compounds such as MnSi and $Fe_{1-x}Co_xSi$, it has recently been found also in an insulating oxide Cu_2OSeO_3 [16]. In common with the B20 transition metal compounds, the space group of the crystal structure is $P2_13$, which is noncentrosymmetric but nonpolar and cubic. Figure 1(a) shows the magnetic phase diagram for Cu_2OSeO_3 [16]. The $S = 1/2$ moments at the Cu^{2+} sites show the local ferrimagnetic arrangement of three-up and one-down type below $T_c \sim 60$ K as observed by powder neutron diffraction [17] and NMR [18] measurements. However, the Dzyaloshinskii-Moriya interaction arising from the noncentrosymmetric lattice structure modulates the ferrimagnetic correlation and induces the helical spin structure with the period of about 60 nm at zero magnetic field [19,20]. While the magnitude of the helical wave vector is determined by the ratio between the asymmetric Dzyaloshinskii-Moriya and symmetric ferrimagnetic interactions, the wave vector direction is nearly degenerate, and the multidomain structure is formed at zero magnetic field [16]. When the magnetic field is applied, the wave vector tends to be aligned along the field direction, forming the single-domain conical spin structure. In a high enough magnetic field, the induced ferrimagnetic state is realized. Just below the critical temperature, on the other hand, there appears the nontrivial magnetic state, i.e., Skyrmion crystal [16]. The real space image of Skyrmion as obtained by Lorentz transmission electron microscopy [16] is reproduced in Fig. 1(b), where the in-plane components of magnetic moments in the Skyrmion are well resolved. Recent neutron diffraction studies also confirm the Skyrmion crystal in bulk Cu_2OSeO_3 crystals [19,20].

Single crystals of Cu_2OSeO_3 were grown by the chemical vapor transport [21] with the same condition as in Ref. [16]. Apart from the effect of the demagnetization field depending on the sample shape (discussed later), the magnetic susceptibility also shows almost the identical behavior. The Skyrmion crystal phase in a bulk crystal is restricted to a narrow range of magnetic field [16,19,20]; therefore, the microwave response can hardly be observed in a conventional ESR spectrometer, in which the probe frequency is fixed and the magnetic resonance is probed by scanning magnetic field. Thus, we have constructed a broadband

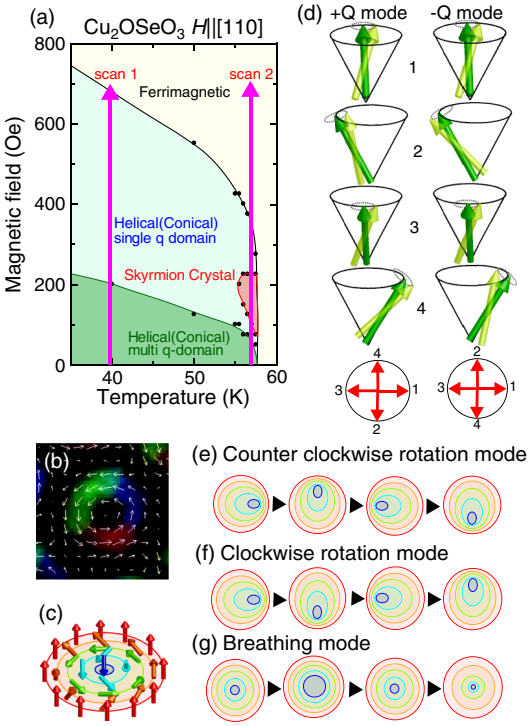

FIG. 1 (color online). (a) Magnetic phase diagram for Cu_2OSeO_3 as determined by the magnetic susceptibility, which is measured with minimal demagnetization field (corresponding to the $H_{DC} \parallel H_{AC}$ configuration in the following microwave experiments). (b) Real-space image of a Skyrmion in Cu_2OSeO_3 obtained by Lorentz transmission electron microscopy, reproduced from Ref. [16]. (c) Schematic illustration of Skyrmion. (d) Illustrations of magnetic excitations in helimagnetic state. The untransparent and half transparent magnetic moments indicate the magnetic moments in static and excited states, respectively. Bottom panel illustrates the oscillating component (the difference between the excited and static states) of magnetic moments in the coordinate system fixed to the static magnetic moment. The numbers stand for the positions of magnetic moments. (e)–(g) Schematic illustrations of magnetic excitations in Skyrmion crystal.

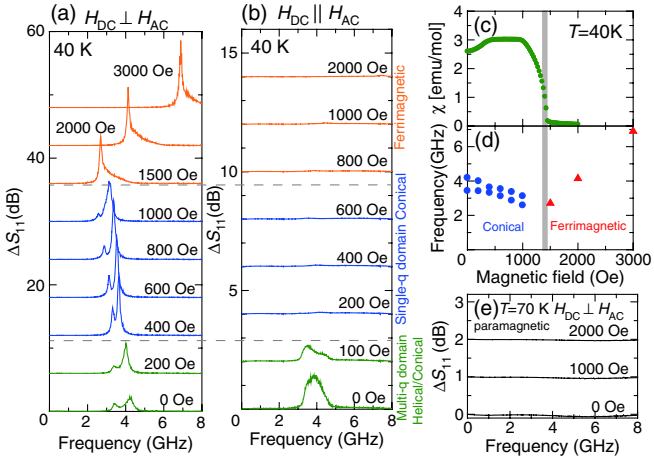

FIG. 2 (color online). (a),(b) Microwave absorption spectra ΔS_{11} at various magnetic fields at 40 K for (a) $H_{DC} \perp H_{AC}$ and (b) $H_{DC} \parallel H_{AC}$. (c) The magnetic field variation of magnetic susceptibility at 40 K measured in the configuration corresponding to the $H_{DC} \perp H_{AC}$ microwave measurement. (d) The magnetic field dependence of the resonance peak frequency in the microwave wave absorption spectra for $H_{DC} \perp H_{AC}$. The closed circles and triangles correspond to the resonant modes in conical magnetic state ($+Q$ and $-Q$ modes) and that in induced ferrimagnetic state, respectively. (e) Microwave absorption spectra ΔS_{11} at various magnetic fields at 70 K for $H_{DC} \perp H_{AC}$.

microwave system with a network analyzer as detailed in Supplemental Material [22]. We have performed the microwave experiment on several crystals and confirmed the qualitatively same result obtained for each crystal. While the pioneering work of electron spin resonance for MnSi was previously done with use of several fixed frequencies [23], our broadband measurement could provide much more information as shown below.

At first, we show the microwave response at 40 K to discuss the magnetic excitations in the helimagnetic state [scan 1 shown in Fig. 1(a)]. In Figs. 2(a) and 2(b), we show the magnetic field dependence of microwave absorption spectra ΔS_{11} at 40 K. (Here, ΔS_{11} stands for the difference of the reflection coefficient S_{11} of the sample-inserted transmission line from the background value, which is proportional to the microwave absorption of the sample; for details, see Supplemental Material [22]). The ac magnetic field of microwave H_{AC} is perpendicular to the dc magnetic field H_{DC} in (a) and parallel in (b). For both cases, H_{DC} is applied along $\langle 110 \rangle$ direction. The microwave spectra are qualitatively unchanged by the variation of H_{DC} direction with respect to the crystal axis in accord with the nearly isotropic phase diagram obtained by Adams *et al.* [19] although they are affected more or less by the static demagnetization field since we used a plate-like sample so as to fit it to the microwave probe. In the configuration of $H_{DC} \parallel H_{AC}$, H_{DC} is parallel to the sample plane and the demagnetization field is small. On the other hand, H_{DC} is perpendicular to the sample plane and the demagnetization field is large in the $H_{DC} \perp H_{AC}$ configuration. Here ΔS_{11} shows two broad peaks around 4 GHz for both $H_{DC} \parallel H_{AC}$ and $H_{DC} \perp H_{AC}$ in the low H_{DC} region. The peaks increase in intensity and become sharper when $H_{DC} = 400$ Oe is applied perpendicular to H_{AC}, whereas they are completely suppressed above 200 Oe in the parallel configuration. As shown in Fig. 1(a), the magnetic wave vector q is aligned along H_{DC} forming a single q domain above 200 Oe. (For the $H_{DC} \perp H_{AC}$ configuration, the critical magnetic field is ~400 Oe because of the large demagnetization field.) Therefore, the contrastive polarization dependence in the high magnetic field indicates that the two magnetic modes can be excited only by H_{AC} perpendicular to the helimagnetic wave vector. Kataoka theoretically identified such two modes in the helical magnetic state induced by Dzyaloshinskii-Moriya interaction [24]. The nature of two modes, $+Q$ mode and $-Q$ mode, is

schematically shown in Fig. 1(d). In the coordinate fixed to the static magnetic moment direction, the oscillating component of $+Q$ mode at a fixed time rotates along the helical wave vector with the period of the static helical spin structure as illustrated in the bottom left panel of Fig. 1(d). In the $-Q$ mode, the rotating period is the same but the direction is opposite. The $+Q$ and $-Q$ modes are almost degenerate but the degeneracy may be lifted by the additional antiferromagnetic interaction [24]. As for the magnetic field dependence in the high field region above 400 Oe, the frequencies of observed two peaks decrease with H_{DC} below 1000 Oe. Above 1500 Oe, only one peak is observed in the measured frequency region, whose frequency rather increases with H_{DC}. In Figs. 2(c) and 2(d), we show the magnetic susceptibility χ and the frequency of the observed peaks in the perpendicular configuration as functions of magnetic field. The magnetic susceptibility is measured in magnetic fields perpendicular to the sample plane corresponding to the $H_{DC} \perp H_{AC}$ configuration. The metamagnetic transition from the conical magnetic state to the induced ferrimagnetic state is observed around 1400 Oe as a kink of magnetic susceptibility. As indicated by a thick gray bar, the change in the observed peak magnetic resonance mode(s) and its (their) field dependence corresponds to this metamagnetic transition. The magnetic field dependence of the mode frequency is in accord with the theoretical result [24], thereby confirming the known character of the magnetic excitations in spin helix. Incidentally, in the paramagnetic state above T_c, magnetic resonance is not discerned at all even under magnetic field, as exemplified by the microwave absorption spectra at 70 K in Fig. 2(e). The signal of electron paramagnetic resonance appears too weak to be clearly observed in the present experimental setup.

Next, we show the newly resolved magnetic resonances in the Skyrmion. We have investigated the magnetic field dependence of microwave absorption spectra at 57.5 K to probe the magnetic excitations in Skyrmion crystal [scan 2 shown in Fig. 1(a)]. In Fig. 3(a), we plot ΔS_{11} for $H_{DC} \perp H_{AC}$ at various magnetic fields. In the low-field helical magnetic state, one broad excitation is observed around 1.8 GHz. The splitting is not clearly observed in this temperature and the frequency is lower than that at 40 K. The peak is unchanged or slightly enhanced with H_{DC} up to 100 Oe. Nevertheless, the helical peak becomes quite weak and alternatively another peak emerges around 1 GHz above 140 Oe. Around 340 Oe, the low-frequency peak disappears and the helical mode revives. In Figs. 3(b)–3(d), we show the frequency and intensity of the peaks as functions of magnetic field, comparing them with the magnetic susceptibility measured in this configuration. The susceptibility shows peaks around 120 and 350 Oe, indicating the phase boundary between the helimagnetic and Skyrmion crystal phases. The field range, where the low-frequency peak is observed, coincides with that for the Skyrmion crystal phase. The intensity of the helical mode

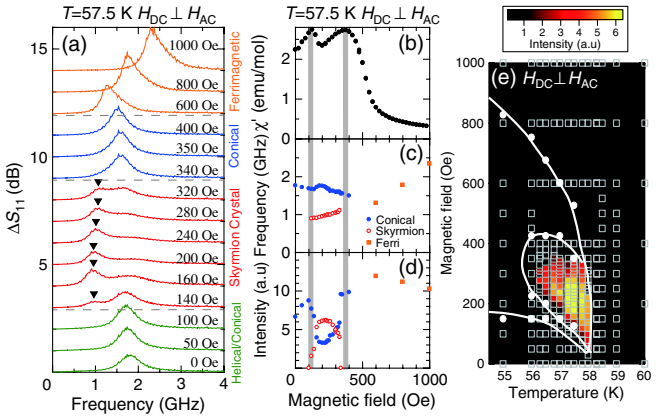

FIG. 3 (color online). (a) The microwave absorption spectra ΔS_{11} for $H_{DC} \perp H_{AC}$ at various magnetic fields at 57.5 K. (b) The magnetic field variation of magnetic susceptibility at 57.5 K measured in the configuration corresponding to the $H_{DC} \perp H_{AC}$ microwave measurement. (c),(d) The (c) frequency and (d) intensity of the magnetic modes in the microwave absorption spectra in (a). The closed and open circles and closed squares in (c),(d) correspond to the excitations in conical magnetic, Skyrmion crystal, and ferrimagnetic states, respectively. (e) The intensity of the magnetic-resonance mode for $H_{DC} \perp H_{AC}$ (counterclockwise rotational mode) in Skyrmion crystal plotted in the H-T phase diagram determined by the magnetic susceptibility measurement. Squares stand for the measured (temperatures, magnetic field) points.

is not completely suppressed even in the Skyrmion crystal phase. A similar coexistence of the helical and Skyrmion crystal states is hinted by the neutron diffraction measurement for B20 compounds (the coexistence of the diffraction spot of $q \parallel H$ due to the helical state and that of $q \perp H$ due to the Skyrmion crystal) [5]. In the induced ferrimagnetic state above 600 Oe, the magnetic susceptibility is suppressed and the peak frequency readily increases with H_{DC}. Figure 3(e) shows the contour mapping of the low-frequency peak intensity in the H-T phase diagram around the Skyrmion-crystal phase determined by the magnetic susceptibility measurement. It is clear from this figure that the low-frequency mode at 1.0 GHz is emergent only in the Skyrmion crystal. Thus, the low-frequency peak is assigned to a magnetic excitation inherent in the Skyrmion crystal.

Figure 4(a) shows the magnetic field variation of ΔS_{11} for $H_{DC} \parallel H_{AC}$ at 57.5 K. The magnetic excitation cannot be excited by the ac magnetic field parallel to the magnetic moment. Note here that, conventional magnetic excitations are usually not observed in this configuration. Nevertheless, we discerned a peak around 1.5 GHz between 50 and 150 Oe. In Figs. 4(b) and 4(d), we plot the frequency and intensity of the peak as well as the magnetic susceptibility measured in this configuration. In the magnetic susceptibility, the sharp peaks are observed at 75 and 250 Oe indicating the phase transition between the conical magnetic and Skyrmion crystal phases. The reason why the

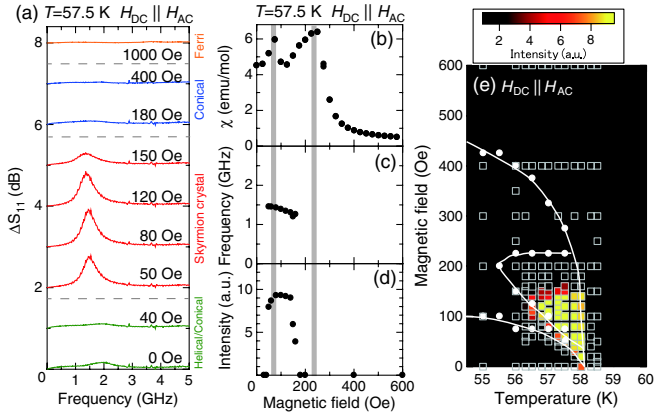

FIG. 4 (color online). (a) The magnetic field dependence of microwave absorption spectra ΔS_{11} for $H_{DC} \parallel H_{AC}$ at 57.5 K. (b) The magnetic field variation of magnetic susceptibility at 57.5 K measured in the configuration corresponding to the $H_{DC} \parallel H_{AC}$ microwave measurement. (c),(d) The (c) frequency and (d) intensity of the magnetic mode in the microwave absorption spectra for $H_{DC} \parallel H_{AC}$. (e) The intensity of the magnetic-resonance mode for $H_{DC} \parallel H_{AC}$ (breathing mode) in Skyrmion crystal plotted in the H-T phase diagram. Squares stand for the measured (temperatures, magnetic field) points.

magnetic field region of Skyrmion crystal phase is lower than that in the $H_{DC} \perp H_{AC}$ configuration is because of the demagnetization field as mentioned previously. The peak around 1.5 GHz is emergent around this magnetic field range. Also for this $H_{AC} \parallel H_{DC}$ configuration, we show the contour mapping of the peak intensity in the magnetic phase diagram determined by the magnetic susceptibility measurement in Fig. 4(e). The region, where the absorption peak is emergent, almost coincides with the Skyrmion crystal phase. [The small difference of the magnetic field (~ 50 Oe) is caused by the artifact, perhaps due to the flux pinning effect in the superconducting magnet.] The microwave absorption peak at 1.5 GHz in this parallel configuration can also be assigned to the excitation in the Skyrmion crystal.

Recently, Mochizuki numerically identified three spin-wave modes in Skyrmion crystal on the basis of Landau-Lifshitz-Gilbert equation [25]. Two modes are counterclockwise and clockwise rotational modes illustrated in Figs. 1(e) and 1(f), in which the core of the Skyrmion rotates in the counterclockwise and clockwise directions, respectively. These modes can be excited by the in-plane H_{AC}. Petrova and Tchernyshyov analytically derived the similar rotational modes [26]. The third mode is the breathing mode shown in Fig. 1(g), in which the core of the Skyrmion expands and shrinks alternately and can be excited by the out-of-plane H_{AC}. Since the Skyrmion plane is always perpendicular to the dc magnetic field, the experimental configurations of $H_{AC} \perp H_{DC}$ and $H_{AC} \parallel H_{DC}$ correspond to the in-plane and out-of-plane H_{AC}, respectively. The observed mode at 1.5 GHz in the $H_{AC} \parallel H_{DC}$ configuration (Fig. 4) can be undoubtedly assigned to the breathing mode of the Skyrmion. For the in-plane polarization ($H_{AC} \perp H_{DC}$), on the other hand, only one Skyrmion mode is experimentally observed while two rotational modes are theoretically anticipated. It is, however, to be noted that the intensity and frequency of the counterclockwise rotational mode are larger and lower, respectively, than those of the clockwise rotational mode according to the theoretical simulation. The experimentally observed mode corresponds perhaps to the intense counterclockwise rotational mode while the higher lying clockwise mode may be mixed with the remaining helical mode and not clearly identified in the experiment.

In summary, we have observed the breathing and rotational modes of Skyrmion in a helimagnet Cu_2OSeO_3. The internal vibrations of Skyrmion should be endowed with the magnetoelectric coupling. Therefore, nontrivial microwave responses such as directional dichroism are expected similarly to electromagnons in the THz regime [27]. In addition, these modes will be useful for the manipulation of Skyrmions as already demonstrated by the numerical calculation [25].

The authors thank M. Mochizuki and N. Nagaosa for fruitful discussion. This work was in part supported by the Grant-in-Aid for Scientific Research (Grant No. 23684023) and by the Japan Society for the Promotion of Science (JSPS) through the "Funding Program for World-Leading Innovative R&D on Science and Technology (FIRST program)," initiated by the Council for Science and Technology Policy (CSTP).

[1] T. H. R. Skyrme, Nucl. Phys. **31**, 556 (1962).
[2] S. L. Sondhi, A. Karlhede, S. A. Kivelson, and E. H. Rezayi, Phys. Rev. B **47**, 16419 (1993).
[3] T.-L. Ho, Phys. Rev. Lett. **81**, 742 (1998).
[4] A. N. Bogdanov and D. A. Yablonskii, Sov. Phys. JETP **68**, 101 (1989).
[5] S. Mühlbauer, B. Binz, F. Jonietz, C. Pfleiderer, A. Rosch, A. Neubauer, R. Georgii, and P. Böni, Science **323**, 915 (2009).
[6] X. Z. Yu, Y. Onose, N. Kanazawa, J. H. Park, J. H. Han, Y. Matsui, N. Nagaosa, and Y. Tokura, Nature (London) **465**, 901 (2010).
[7] X. Z. Yu, N. Kanazawa, Y. Onose, K. Kimoto, W. Z. Zhang, S. Ishiwata, Y. Matsui, and Y. Tokura, Nature Mater. **10**, 106 (2010).
[8] F. Jonietz *et al.*, Science **330**, 1648 (2010).
[9] T. Schulz, R. Ritz, A. Bauer, M. Halder, M. Wagner, C. Franz, C. Pfleiderer, K. Everschor, M. Garst, and A. Rosch, Nature Phys. **8**, 301 (2012).
[10] X. Z. Yu, N. Kanazawa, W. Z. Zhang, T. Nagai, T. Hara, K. Kimoto, Y. Matsui, Y. Onose, and Y. Tokura, Nature Commun. (to be published).
[11] A. P. Malozemoff and J. C. Slonczewski, *Magnetic Domain Walls in Bubble Materials* (Academic, New York, 1979).
[12] M. Lee, W. Kang, Y. Onose, Y. Tokura, and N. P. Ong, Phys. Rev. Lett. **102**, 186601 (2009).

[13] A. Neubauer, C. Pfleiderer, B. Binz, A. Rosch, R. Ritz, P. G. Niklowitz, and P. Böni, Phys. Rev. Lett. **102**, 186602 (2009).
[14] N. Kanazawa, Y. Onose, T. Arima, D. Okuyama, K. Ohoyama, S. Wakimoto, K. Kakurai, S. Ishiwata, and Y. Tokura, Phys. Rev. Lett. **106**, 156603 (2011).
[15] J. Zang, M. Mostovoy, J. H. Han, and N. Nagaosa, Phys. Rev. Lett. **107**, 136804 (2011).
[16] S. Seki, X. Z. Yu, S. Ishiwata, and Tokura, Science **336**, 198 (2012).
[17] Jan-Willem G. Bos, C. V. Colin, and T. T. M. Palstra, Phys. Rev. B **78**, 094416 (2008).
[18] M. Belesi, I. Rousochatzakis, H. C. Wu, H. Berger, I. V. Shvets, F. Mila, and J. P Ansermet, Phys. Rev. B **82**, 094422 (2010).
[19] T. Adams, A. Chacon, M. Wagner, A. Bauer, G. Brandl, B. Pedersen, H. Berger, P. Lemmens, and C. Pfleiderer, Phys. Rev. Lett. **108**, 237204 (2012).
[20] S. Seki, J.-H. Kim, D. S. Inosov, R. Georgii, B. Keimer, S. Ishiwata, and Y. Tokura, Phys. Rev. B **85**, 220406(R) (2012).
[21] K. H. Miller, X. S. Xu, H. Berger, E. S. Knowles, D. J. Arenas, M. W. Meisel, and D. B. Tanner, Phys. Rev. B **82**, 144107 (2010).
[22] See Supplemental Material at http://link.aps.org/supplemental/10.1103/PhysRevLett.109.037603 for details about the experimental setup of microwave absorption.
[23] M. Date, K. Okuda, and K. Kadowaki, J. Phys. Soc. Jpn. **42**, 1555 (1977).
[24] M. Kataoka, J. Phys. Soc. Jpn. **56**, 3635 (1987).
[25] M. Mochizuki, Phys. Rev. Lett. **108**, 017601 (2012).
[26] O. Petrova and O. Tchernyshyov, Phys. Rev. B **84**, 214433 (2011).
[27] Y. Takahashi, R. Shimano, Y. Kaneko, H. Murakawa, and Tokura, Nature Phys. **8**, 121 (2011).